ACS APPLIED POLYMER MATERIALS

pubs.acs.org/acsapm

Article

Photopolymers Based on Boronic Esters for the Enhanced Degradation of 3D-Printed Scaffolds

Lisa Sinawehl, Raffael Wolff, Thomas Koch, Jürgen Stampfl, Robert Liska, and Stefan Baudis*

Cite This: *ACS Appl. Polym. Mater.* 2023, 5, 5758−5771

Read Online

ACCESS | Metrics & More | Article Recommendations | Supporting Information

ABSTRACT: Lithography-based additive manufacturing technologies have become a valuable tool in tissue engineering for the fabrication of biocompatible and biodegradable bone regeneration scaffolds. Currently employed photopolymers based on (meth)acrylates, vinyl esters, or vinyl carbonates display undesirable properties such as irritancy or cytotoxicity of residual monomers, degradation via autocatalytic bulk erosion leading to implant failure, or insufficient degradation speed *in vivo*. This work investigates monomers containing boronic ester bonds as a potential alternative to these state-of-the-art compounds. Next to a facile synthesis, significantly lower cytotoxicity was shown for this generation of biocompatible allyl ether monomers compared to commonly utilized (meth)acrylates. Photopolymerization via the thiol−ene reaction showed that rigid boronic esters led to sufficient photoreactivity for 3D structuring, and materials with reduced shrinkage and excellent mechanical properties can be obtained. Additionally, degradation studies revealed significantly accelerated degradation via the desired surface erosion under physiological and acidic conditions. Ultimately, a 3D test structure out of a boronic ester-based formulation was successfully stereolithography-printed, showing the great potential of these monomers as precursors for photopolymers used for 3D-printed implants with improved degradation behavior without forfeiting good mechanical properties.

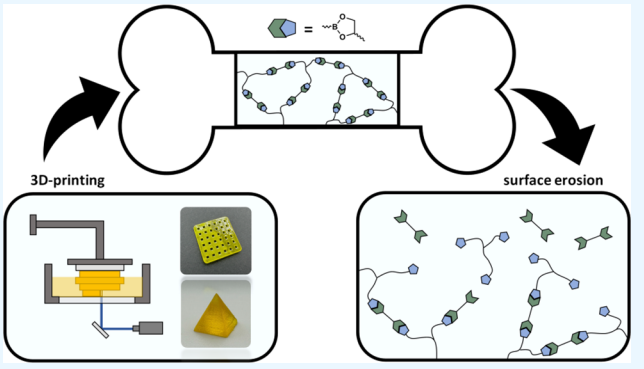

KEYWORDS: *biomaterials, stereolithography, photopolymerization, tissue regeneration, bone regeneration*

1. INTRODUCTION

In recent years, significant progress has been made in additive manufacturing technologies (AMTs) to produce cellular objects with defined geometry.[1,2] Since then, these methods have become an appealing approach to generating biocompatible and biodegradable 3D scaffolds as temporary support structures in tissue engineering (TE) and regenerative therapy.[3] Especially, lithography-based AMTs (L-AMTs), such as stereolithography (SLA) or digital light processing (DLP), received increasing interest because high surface quality and feature resolutions down to 10 μm can be obtained due to the selective irradiation of photosensitive resins in a layer-by-layer process. In the case of bone tissue engineering (BTE), L-AMTs were shown to be ideal for producing complex regeneration scaffolds with defined porosities, which can be tailored specifically to each patient. Furthermore, it was shown that surface topology and feature sizes were beneficial for subsequent bone regeneration.[4,5]

Biocompatible and biodegradable poly(lactic acid) and poly(caprolactone), the most often employed materials used in TE, cannot be processed by these light-based techniques and degrade in the order of years under physiological conditions, which is too slow for BTE applications.[6,7] Furthermore, currently employed state-of-the-art (meth)acrylate-based photopolymers suffer from adverse effects, such as irritancy or even cytotoxicity of residual monomers.[8,9] Additionally, upon degradation, high-molecular-weight poly[(meth)acrylic acids] are formed, which cannot be removed from the body and promote inflammation or tissue necrosis. They further cause autocatalytic bulk erosion of the material with a rapid loss of mechanical strength.[6,8,10,11]

Recently, vinyl esters and vinyl carbonates emerged as potent alternatives to (meth)acrylic resins in terms of drastically decreased cytotoxicity.[3,9,10,12−15] Nevertheless, similar to classical (meth)acrylate, formed polymers tend to be very brittle and break during polymerization owing to the high volumetric shrinkage. This limits their use in materials for regeneration scaffolds, which require certain mechanical properties for good load dissipation and tissue integration.[8] In general, depending on the specific composition and the structure of the replaced bony tissue, a tensile strength ranging

Received: May 23, 2023
Accepted: June 12, 2023
Published: June 29, 2023

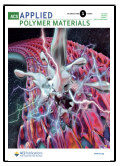

from 10 to 150 MPa, an elongation of 1−7%, and a toughness of 2−12 J/m^3 of the substitute material are crucial.[16] To circumvent the problems regarding the mechanical properties, chain-transfer agents such as thiols can be employed, resulting in more homogeneous networks with sharpened glass transition temperatures, lower shrinkage stress, and high fracture toughness.[17−20] Additionally, upon thiol addition, an increase in the monomer reactivity was observed due to suppressed intermolecular hydrogen abstraction and reduced oxygen inhibition.[14] Although first *in vivo* studies confirmed good biocompatibility of the photopolymers and no autocatalytic bulk erosion of implanted scaffolds, the degradation of all polymers occurred in the order of years; hence, rates were found to be insufficient to match the rate at which bone tissue regenerates.[1,3,9,10] Accordingly, novel biocompatible monomers are required in BTE, which form polymers with accelerated degradation *in vivo*. Although dependent on the type and location of the replaced bone tissue and the specific patient, degradation of scaffolds should be exhibited within 3−12 months to enable tissue remodeling and vascularization.[16,21−23] Furthermore, ideally, degradation should occur via surface erosion, during which the loss of the material is confined to the surface, preventing premature implant failure.[6,24]

In literature, examples of labile bonds used to enhance network degradation include orthoesters,[25] anhydrides,[3] acetals,[26] and ketals.[27] Boronic esters are commonly utilized as environmentally benign, easily prepared, and low-cost reagents for Suzuki−Miyaura couplings and are generally renowned for their low cytotoxicity.[28,29] Furthermore, they are known to be readily hydrolyzed, yielding a boronic acid and an alcohol. As mild organic Lewis acids with low toxicity and ultimate degradation into boric acid, boronic acids are regarded as "green" compounds and do not lead to drastic pH changes in the surrounding medium.[7,28−30]

Due to the reversibility of the ester hydrolysis and their unique feature of catalyst-free transesterification reactions, boronic esters have been widely utilized to prepare dynamic materials in solution-based systems, such as molecular sensors and drug-delivery systems.[31−35] Recently, Leibler et al.[36] and Guan et al.[37] reported dynamic exchange reactions of boronic esters in bulk polymers resulting in network rearrangement. Since then, boronic ester bonds have been extensively studied in materials capable of self-healing, reshaping, and recycling.[30,32,37−41] Tajbakhsh et al. report the synthesis of recyclable, cross-linked networks containing boronic ester bonds.[42] According to Guo et al., self-healable, malleable, and reprocessable, cross-linked rubbers were successfully prepared by the incorporation of boronic ester bonds.[43,44] Sumerlin et al. describe self-healing of cross-linked boronic ester networks formed via radical-initiated thiol−ene polymerization.[40,41] In AMTs, boronic esters have been frequently employed to produce self-healable hydrogels via extrusion.[45,46] Very recently, Sample et al. reported the first DLP printing of dynamic networks based on boronic esters, which were also capable of self-healing.[47] Additionally, the ability of networks to undergo hydrolysis in the presence of water was reported. However, due to the low glass transition temperature of the polymers, the addition of a monomer without dynamic bonds was necessary to prevent creep and failure during printing, and significant swelling of >100% of the resulting networks was observed.[39,48,49] Accordingly, there is still no literature on polymers containing boronic ester bonds shaped by AMTs with mechanical properties sufficient for the replacement of human bone and degradation via surface erosion.

Therefore, the focus of this present work was to synthesize photopolymers with enhanced degradation characteristics compared to state-of-the-art poly(meth)acrylates with a possible application as biocompatible and biodegradable bone regeneration scaffolds. We envisioned that, due to the facile hydrolysis and the absence of highly acidic hydrolysis products, the boronic ester functionality would be well suited to generate materials with favorable degradation via surface erosion. Additionally, we hypothesized that, by using a rigid boronic ester monomer in combination with a rigid thiol, polymers with good mechanical properties would be formed that do not display undesired creep during printing. Finally, due to the enhanced mechanical properties of the polymers, we hypothesized that 3D printing of boronic ester-based formulations without the addition of monomers not containing boronic ester bonds would be possible in order to generate 3D-printed scaffolds with degradable bonds at every cross-linking point. By this, low-molecular-weight, water-soluble hydrolysis products should be formed, which can be metabolized or excreted from the body. Therefore, boronic ester monomers were synthesized and polymerized in bulk with radical-initiated thiol−ene photopolymerization. All used monomers and thiols were investigated regarding cytotoxicity toward mouse fibroblast cells to confirm their applicability in biomedical fields. Because photocuring rates are a prerequisite for successful structuring, formulations were analyzed regarding photoreactivity. The mechanical properties of the resulting bulk networks were characterized, and the degradation behavior was determined. Finally, SLA printing of the best-performing formulation was conducted to elucidate the potential of these monomers in BTE applications.

2. EXPERIMENTAL SECTION

2.1. Reagents and Materials. 1,3,5-Triallyl-1,3,5-triazine-2,4,6-trione (TCI, 98%), thioacetic acid (TCI, > 95%), 4-vinyl-1,3-dioxolan-2-one (TCI, >98%), benzene-1,4-diboronic acid (ABCR, 96%), 3-allyloxy-1,2-propanediol (TCI, >99%), 3,9-divinyl-2,4,8,10-tetraoxaspiro[5.5]undecane (TCI, 98%), and molecular sieves (4 Å, Sigma-Aldrich) were purchased from respective companies and used as received unless otherwise noted. 2,2′-Azobis(2-methylpropionitrile) (AIBN; Sigma-Aldrich, 98%) was recrystallized from distilled methanol (MeOH) at room temperature (rt). Commercial-grade MeOH (Donau Chemie), tetrahydrofuran (THF; Donau Chemie), and dioxane (Donau Chemie) were dried with a PureSolv system (Inert, Amesbury, MA). Chloroform-*d* ($CDCl_3$; Eurisotop, 99.8%) was dried overnight over 4 Å molecular sieves. The photoinitiator bis(4-methoxybenzoyl)diethylgermanium (Ivocerin) was kindly provided by Ivoclar Vivadent AG and used as received.

2.2. Synthesis of 1,3,5-Tris(3-acetylmercaptopropyl)-1,3,5-triazine-2,4,6-trione (TAT). The product was synthesized as described by Reinet et al.[50,51] In a 1000 mL three-neck round-bottomed flask, 1,3,5-triallyl-1,3,5-triazine-2,4,6-trione (80.0 g, 1 equiv, 321 mmol), thioacetic acid (87.9 g, 3.6 equiv, 1155 mmol), and AIBN (7.9 g, 0.15 equiv, 48 mmol) were dissolved in 1000 mL of THF. The reaction mixture was purged with argon for 30 min at rt and then heated to 65 °C for 24 h. After cooling to 0 °C, 200 mL of 1 N Na_2CO_3 was added, and the mixture was extracted three times with dichloromethane (DCM; 600/200/200 mL). The combined organic extracts were washed with 160 mL of 1 N aqueous NaOH and 160 mL of brine, dried over Na_2SO_4, filtered, and concentrated under reduced pressure to obtain the crude product as a dark-yellow solid. The crude product was recrystallized from ∼200 mL of MeOH three times to yield the product as a white solid in a yield of 110.4 g (72% calculated yield). Mp: 65−68 °C (lit.[51] 64−66 °C). ^{1}H NMR (400

https://doi.org/10.1021/acsapm.3c01000
ACS Appl. Polym. Mater. 2023, 5, 5758−5771

MHz, $CDCl_3$): δ 3.89 (t, J = 7.1 Hz, 6H, −N−CH_2−), 2.83 (t, J = 7.1 Hz, 6H, −CH_2S−), 2.26 (s, 9H, −CH_3), 1.87 (quin., J = 7.1 Hz, 6H, −CH_2−). ^{13}C NMR (101 MHz, $CDCl_3$): δ 195.45 (−S(C═O)CH_3), 149.03 (−C═O), 42.07 (−N−CH_2−), 30.68 (−CH_3), 28.03 (−CH_2−), 26.27 (−CH_2−S−).

2.3. Synthesis of 1,3,5-Tris(3-mercaptopropyl)-1,3,5-triazine-2,4,6-trione (TMT). To synthesize the corresponding thiol, TMT, TAT (110.0 g, 1 equiv, 230 mmol), and aqueous concentrated HCl (26.9 g, 3.2 equiv, 737 mmol) was dissolved in a mixture of MeOH (460 mL) and 1,4-dioxane (150 mL). The resulting solution was purged with argon for 30 min and then heated to 60 °C for 24 h. After cooling to ambient temperature, 500 mL of deionized water was added, and the mixture was extracted three times with DCM (600/400/400 mL). The combined organic extracts were washed two times with 250 mL of saturated $NaHCO_3$ and brine, dried over Na_2SO_4, filtered, and concentrated under reduced pressure to yield the pure product as a colorless liquid in a yield of 75.3 g (93% calculated yield). n_D^{20} = 1.5678. ^{1}H NMR (400 MHz, $CDCl_3$): δ 4.01 (t, J = 7.0 Hz, 6H, −N−CH_2−), 2.56 (dt, J = 6.9 and 8.0 Hz, 6H, −CH_2S−), 1.97 (quin, J = 7.0 Hz, 6H, −CH_2−), 1.54 (t, J = 8.0 Hz, 3H, −CH_2−SH). ^{13}C NMR (101 MHz, $CDCl_3$): δ 149.10 (−C═O), 41.91 (−N−CH_2−), 31.94 (−CH_2−), 22.03 (−CH_2−SH).

2.4. Synthesis of But-3-ene-1,2-diol. The alcohol was synthesized according to Boaz et al.[52] Therefore, 4-vinyl-1,3-dioxolan-2-one (79.9 g, 1 equiv, 700 mmol) was added to a 1000 mL three-neck flask and cooled to 0 °C with an ice bath. Then, a 50 wt % solution of aqueous KOH (45.2 g, 1,15 equiv, 805 mmol) was added dropwise over a period of 1 h. After complete addition, the ice bath was removed and the mixture was heated to 60 °C for 16 h. After the mixture was cooled to ambient temperature, 370 mL of isopropyl alcohol (i-PrOH) was added, and the mixture was stirred for 1 h. The precipitated salt was filtered off and washed with 50 mL of i-PrOH. The organic phase was concentrated *in vacuo* to yield the crude product as a colorless liquid. Purification was conducted by distillation at 10 mbar and 90 °C to yield the pure product as a colorless oil in a yield of 49.3 days (80% calculated yield). n_D^{20} = 1.4615. ^{1}H NMR (400 MHz, $CDCl_3$): δ 5.84 (ddd, J = 17.3, 10.6, and 5.6 Hz, 1H, −CH═), 5.35 (dt, J = 17.3 and 1.5 Hz, 1H, ═CH_2), 5.21 (dt, J = 10.6 and 1.4 Hz, 1H, ═CH_2), 4.25 (ddtq, J = 7.5, 4.3, 3.2, and 1.5 Hz, 1H, −CH−OH), 3.66 (ddd, J = 11.3, 6.8, and 3.4 Hz, 1H, −CH_2OH), 3.49 (ddd, J = 11.3, 7.5, and 4.9 Hz, 1H, −CH_2OH), 3.01 (d, J = 4.3 Hz, 1H, −OH), 2.84 (dd, J = 6.8 and 5.0 Hz, 1H, −OH). ^{13}C NMR-APT (101 MHz, $CDCl_3$): δ 136.71 (−CH═), 116.75 (═CH_2), 73.32 (−CH−OH), 66.25 (−CH_2OH).

2.5. Synthesis of 1,4-Bis(4-vinyl-1,3,2-dioxaborolan-2-yl)-benzene (Vinyldioxaborolane, VDB). The synthesis was conducted according to a modified procedure from Chen et al.[43,44] Therefore, benzene-1,4-diboronic acid (33.2 g, 1 equiv, 200 mmol) and but-3-ene-1,2-diol (36.1 g, 2.05 equiv, 410 mmol) were added to a 2000 mL flask under an inert atmosphere and completely dissolved in 1000 mL of THF by stirring for ∼30 min. Then Na_2SO_4 (65.1 g, 2.3 equiv, 458 mmol) was added stepwise to the solution. After being stirred at rt for 16 h, Na_2SO_4 was filtered off, and the filtrate was concentrated *in vacuo* to obtain the pure solid product as a white solid in quantitative yield. Mp: 73−74.9 °C. ^{1}H NMR (400 MHz, $CDCl_3$): δ 7.85 (s, 4H, −C−H_{Ar}), 5.96 (ddd, J = 17.0, 10.4, and 6.6 Hz, 2H, −CH═), 5.41 (dt, J = 17.1 and 1.3 Hz, 2H, ═CH_2), 5.27 (dt, J = 10.3 and 1.2 Hz, 2H, ═CH_2), 5.02 (dddt, J = 8.5, 7.7, 6.6, and 1.2 Hz, 2H, −O−CH−), 4.51 (dd, J = 9.1 and 8.2 Hz, 2H, −O−CH_2−), 4.05 (dd, J = 9.0 and 7.4 Hz, 2H, −O−CH_2−) (Figure S1). ^{13}C NMR-APT (101 MHz, $CDCl_3$): δ 137.10 (−CH═), 134.28 (−C−H_{Ar}), 117.59 (═CH_2), 78.47 (−O−CH−), 71.17 (−O−CH_2−) (Figure S2). ^{11}B NMR (128 MHz, $CDCl_3$): δ 31.22 (Figure S3).

2.6. Synthesis of 1,4-Bis[4-(allyloxy)methyl-1,3,2-dioxaborolan-2-yl]benzene (Allyldioxaborolane, ADB). The synthesis was conducted analogously to Chen et al. and Robinson et al.[43,44,47] Therefore, 3-allyloxy-1,2-propanediol was distilled prior to the synthesis for purification (bp: 105 °C at 3 mbar). Benzene-1,4-diboronic acid (13.2 g, 1 equiv, 80 mmol) and 3-allyloxy-1,2-propanediol (21.7 g, 2.05 equiv, 164 mmol) were added to a 1000 mL three-neck round-bottomed flask under an inert atmosphere and dissolved completely in 450 mL of THF by stirring for ∼30 min. Then, Na_2SO_4 (26.0 g, 2.3 equiv, 183 mmol) was added stepwise to the solution, which was then stirred for 16 h at rt. Then, Na_2SO_4 was filtered off, and the filtrate was concentrated *in vacuo* to obtain the pure solid product as an off-white solid in quantitative yield. Mp: 42−43 °C. ^{1}H NMR (400 MHz, $CDCl_3$): δ 7.83 (s, 4H, −C−H_{Ar}), 5.89 (ddt, J = 17.2, 10.4, and 5.6 Hz, 2H, −CH═), 5.28 (dq, J = 17.2 and 1.6 Hz, 2H, ═CH_2), 5.19 (dq, J = 10.4 and 1.4 Hz, 2H, ═CH_2), 4.74 (ddt, J = 8.1, 6.6, and 5.1 Hz, 2H, −O−C<u>H</u>−CH_2−), 4.43 (dd, J = 9.1 and 8.2 Hz, 2H, −O−CH−C<u>H</u>$_2$−), 4.19 (dd, J = 9.1 and 6.6 Hz, 2H, −C<u>H</u>$_2$−CH═), 4.07 (dq, J = 5.6 and 1.4 Hz, 4H, −O−C<u>H</u>$_2$−CH), 3.64 (dd, J = 10.2 and 5.1 Hz, 2H, −O−C<u>H</u>$_2$−CH═), 3.57 (dd, J = 10.2 and 5.1 Hz, 2H, −O−CH−C<u>H</u>$_2$−O−). ^{13}C NMR (101 MHz, $CDCl_3$): δ 136.95 (−C_{Ar}), 134.36 (−CH═), 134.11 (−C−H_{Ar}), 117.47 (═CH_2), 76.22 (−O−<u>C</u>H−CH_2−), 72.58 (−O−<u>C</u>H$_2$−CH═), 71.91 (−O−CH−<u>C</u>H$_2$−O−), 68.51 (−O−<u>C</u>H$_2$−CH−). ^{11}B NMR (128 MHz, $CDCl_3$): δ 31.50.

2.7. Preparation of Formulations. All formulations were prepared in an orange-light laboratory, with wavelengths below 480 nm filtered out to avoid light contact. Formulations consisted of each monomer and the thiol TMT in a 1:1 molar ratio of vinyl-to-thiol groups of 1:1. All polymerizations were carried out in bulk without solvent by photopolymerization. As a radical photoinitiator, 1 wt % Ivocerin was used. Pyrogallol (PYR; 0.02 wt %) was added for stabilization. The samples containing the reference monomer 3,9-divinyl-2,4,8,10-tetraoxaspiro[5.5]undecane (vinylspiroacetal, VSA) and the boronic ester ADB were homogenized with a vortex under slight heating until homogeneous and bubble-free solutions were obtained. The formulation with VDB was stored in a drying oven at 90 °C for 10 min before vortexing to fully dissolve the solid monomer and was subsequently stored in a drying oven at 50 °C before further analysis and curing to prevent reprecipitation of the monomer.

2.8. Characterizations. *NMR Spectra.* NMR spectra were recorded at rt on a Bruker Avance at 400 MHz for ^{1}H NMR, 101 MHz for ^{13}C NMR, and 128 MHz for ^{10}B NMR. The samples were dissolved in $CDCl_3$ and referenced to the solvent residual peak. Chemical shifts are given in parts per million, multiplicities are termed s (singlet), d (doublet), t (triplet), q (quartet), and m (multiplet), and coupling constants (J values) are given in hertz. The data were processed with the software *TopSpin 3.5 pl 7* from Bruker.

Evaluation of Cytotoxicity. In vitro cytotoxicity of the monomers and the thiol TMT was tested in NCTC Clone 929 fibroblast cell culture using a Presto Blue assay. The cells were cultured in Dulbecco's modified eagle medium (DMEM) supplemented with 10% fetal bovine serum (FBS) and penicillin−streptomycin (100 U/mL penicillin and 100 μg/mL streptomycin) in 96-well plates at a density of 1 × 10^4 cells/well for 24 h in humidified air with 95% relative humidity and with 5% CO_2 at 37 °C. The tested substances were dissolved in dimethyl sulfoxide (DMSO) to obtain 1 M solutions. These solutions were then further diluted with DMEM, 10% FBS, 100 U/mL penicillin, and 100 μg/mL streptomycin to produce solutions with four different concentrations (0.01, 0.0075, 0.005, and 0.0025 mol/L). After 24 h, the cells were treated with 100 μL of each solution in triplicate and incubated at 37 °C for 24 h. Qualitative screening of morphological changes was conducted under the microscope according to ISO 10993-5. For quantitative screening of the cell viability, the supernatant solution was removed, and 10 μL of resazurin was added to the cells. After 1 h at 37 °C, the fluorescence intensity was measured at 570 nm. As control values, cells treated with a 1% DMSO solution, a blank value, and phosphate-buffered saline (PBS) buffer were used. The results represent the mean of the triplicate measurements. For evaluation, the viability of the negative control was assumed to be 100% and the background fluorescence was subtracted from each measurement signal. For calculation of the viability of the treated cells, the mean of the treated cells was divided by the mean of the control culture on the respective cell culture plate. The concentration at which 50% of the cells are still viable after 1 day was used to determine the cytotoxicity.

https://doi.org/10.1021/acsapm.3c01000
ACS Appl. Polym. Mater. 2023, 5, 5758−5771

Viscosity Measurements. Rheology measurements of all prepared formulations were conducted on the modular compact rheometer MCR 300 by Physica Anton Paar. A total of 75−80 μL of the freshly prepared formulations was used for the measurements. After 5 min of acclimatization time, the viscosity of the formulations was measured at 25 or 100 °C with a CP25 (cone plate) measuring system with a diameter of 25 mm, a gap of 48 μm, and a constant shear rate of 100 s^{-1}.

Real-Time Near-Infrared (RT-NIR) Photorheology. Measurements were performed with a RT-NIR photorheometer consisting of an Anton Paar MCR 302 WESP with a P-PTD 200/GL Peltier glass plate and a PP25 measuring system coupled with a Bruker Vertex 80 Fourier transform infrared spectrometer. An external mirror was used to guide the IR beam from the spectrometer through the glass plate and from the sample to the rheology plate, which reflected the beam. The beam was detected with an external mercury−cadmium−telluride detector. A total of 150−180 μL of all tested monomer formulations was placed at the center of the glass plate, which was covered with polyethylene tape (TESA 4668 MDPE) for smooth sample removal. Measurements were conducted at 25 °C for the formulation containing VSA or ADB or at 55 °C for the formulation containing VDB with an Anton Paar H-PTD 200 furnace and a gap of 200 μm. The samples were sheared with a strain of 1% and a frequency of 1 Hz. During the measurement, storage and loss moduli were recorded. To start photopolymerization, irradiation was conducted for 320 s with a waveguide from below the glass plate using an Exfo OmniCureTM 2000 with a broadband mercury lamp equipped with a 400−500 nm filter. An intensity of 1 W/cm^2 was used at the tip of the light guide, corresponding to an intensity of 20 mW/cm^2 at the surface of the samples. Irradiation was induced 65 s after the start of each measurement. The IR chamber was continuously purged with dry air. The measurements were performed with each formulation in triplicate with a closed furnace. The double-bond conversion (DBC) over time was determined by recording an IR spectra every 0.2 s and then integrating the respective double-bond bands at ∼6170 cm^{-1}. The double-bond peak area ratio at the start and end of the measurement yielded DBC. The rate of polymerization (R_p) of the formulations was determined by the linear regression of the DBC curves at the start of the measurements.

Preparation of Cross-Linked Networks. The curing of the samples was conducted in transparent silicone molds without a lid. For dynamic mechanical thermoanalysis (DMTA) measurements, specimens with dimensions of 2 × 5 × 40 mm^3, and for tensile testing, bone-shaped specimens of shape 5B according to ISO527-2:2019 were prepared. For degradation studies, cylindrically shaped specimens with dimensions of d = 6 mm and h = 2 mm and a mass of approximately 50 mg were cured. Curing was conducted in a Lumamat 100 light oven with six Osram Dulux L Blue 18 W lamps. The emitted wavelength spectrum of this oven ranges from 400 to 580 nm at a measured total intensity of ∼20 mW/cm^2. The formulations containing VSA and ADB were cured at rt, while the formulation containing VDB was cured with a special curing program in which the samples are heated to ∼54 °C during curing. All samples were cured on both sides for 10 min and then sanded to remove surface imperfections. All specimens were subsequently stored under dry conditions and an argon atmosphere until testing.

DMTA. DMTA measurements were performed with an Anton Paar MCR 302e device with a CTD 450 oven and a SRF 12 measuring system. The fabricated specimens were tested in torsion mode with a frequency of 1 Hz and a torsion strain of 0.1%. The temperature was increased from −100 to +200 °C with a heating rate of 2 K/min. The storage modulus and loss factor of the polymer samples were recorded with the software *RheoCompass 1.24* from Anton Paar. The glass transition temperature was determined via the maximum of the loss factor (tan δ). Due to the high reproducibility of this method, specimens were tested once.

Tensile Tests. Tensile tests were conducted on a Zwick Z050 tensile testing machine equipped with a 1 kN load sensor. The crosshead speed was set to 5 mm/min, and the strain was calculated from the crosshead travel and the parallel length of the specimen. To guarantee reproducibility, five replicates were measured per material. Analysis was performed using *TestXpert II* testing software. Because no extensometer was used, the slope in the linear regimen of the curve was used to evaluate the stiffness of the material.

In Vitro Degradation of Cross-Linked Networks. Degradation studies were conducted in buffered conditions under acidic conditions (acetate buffer, pH 4) as well as conditions present in the body (PBS, pH 7.4). The PBS solution was fabricated with 8.0 g of NaCl, 0.2 g of KCl, 1.44 g of Na_2HPO_4, and 0.24 g of KH_2PO_4 in 1 L of distilled water. The acetate buffer was prepared with 5.77 g of sodium acetate and 1.78 g of acetic acid dissolved in 1 L of distilled water. Also, degradation under basic conditions was studied (see the Supporting Information, SI). The initial mass of the samples was measured with a balance of 0.01 mg precision. Each sample was immersed in 15 mL of the respective buffer medium and stored in a climate chamber at 37 °C. After 2, 7, 14, 21, 30, and 60 days, three samples of each material and each condition were removed from the buffer solution, the surface of the polymer was gently dried using an absorbent wipe, and each sample was weighed directly for determination of the swelling, which was calculated as the mass change from swollen mass to the degraded mass after drying, normalized to the degraded mass after drying (eq S1). The removed samples were washed with deionized water and then put back into the empty vial, which was washed with deionized water. The samples were dried to a constant weight in a drying oven at 50 °C. For the sake of consistency, all dried samples were weighed with the vial because some were disrupted during the experiment or became too fragile for removal. The mass change was calculated as the mass change from the original mass to degraded mass after drying, normalized to the degraded mass (eq S1). The determined data represent the average of three samples at each time point. At regular intervals, the pH of the buffer medium was checked to ensure constant degradation conditions. After 3 M, each buffer solution was extracted with 0.7 mL of $CDCl_3$ and NMR measurements were conducted to study the hydrolysis products and residues in the vials.

Sterilization of Networks. For sterilization studies, tensile test specimens of the material containing monomer VDB and thiol TMT were prepared. Sterilization of all samples was conducted by the KLS Martin Group. Sterilization with ethylene oxide (EO) was conducted according to DIN EN ISO 11135-1 with a concentration of 6% EO in CO_2 for 2 h at 55 °C, followed by a 6 h desorption phase. Sterilization with γ radiation was done using a ^{60}Co radiation source for 5 h with either a low radiation dose of 18.6 kGy or a high dose of 30.5 kGy according to DIN EN ISO 9001, DIN EN ISO 13485, and DIN EN ISO 11137-1.

3D Printing. 3D structuring of the resin containing the monomer VDB and the thiol TMT was performed on a Caligma 200 UV prototype with a bottom-up SLA setup.[53] The formulation contained an equimolar amount of vinyl-to-thiol groups, 1 wt % Ivocerin, and 0.02 wt % PYR. For control over the spatial resolution and curing depth, 0.1 wt % absorber Quinoline Yellow (QY) was added. The vat and building platform of the printer were heated to 55 °C during the printing process. Production of the structures was conducted by scanning a laser beam over a 2D plane using a Galvano scanner. An irradiation wavelength of 375 nm and a power of 70 mW/mm^2 were used. The diameter of the laser spot during printing was 25 μm. A writing speed of 100 mm/s and a layer thickness of 100 μm were applied.

3. RESULTS AND DISCUSSION

Biocompatible and biodegradable, patient-specific regeneration scaffolds fabricated by L-AMTs represent the future of TE and are urgently needed because the human body is incapable of repairing larger bone defects caused by trauma or diseases.[54] For good osseointegration, high tensile strength, glass transition temperature, and toughness of the 3D-printed scaffolds are crucial.[8] Because state-of-the-art (meth)acrylic resins lack satisfying mechanical properties and degrade too slowly via bulk erosion, alternative monomers are required.[10,15]

https://doi.org/10.1021/acsapm.3c01000
ACS Appl. Polym. Mater. 2023, 5, 5758−5771

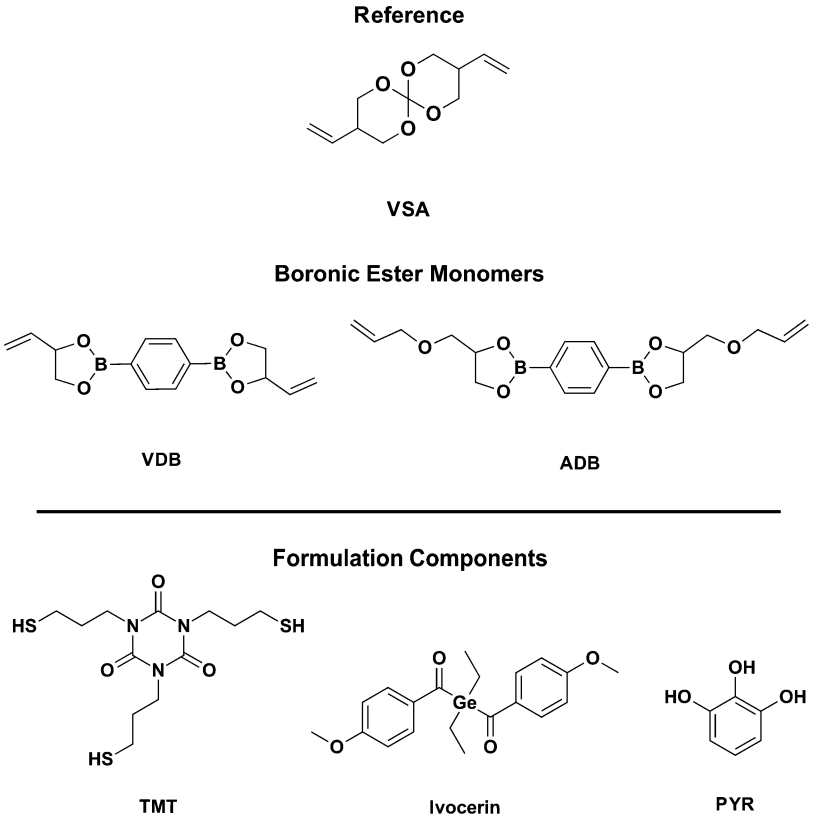

Figure 1. Schematic representation of the following compounds: reference VSA, novel boronic ester monomer VDB, and boronic ester monomer ADB. Further formulation components are the thiol TMT, the photoinitiator Ivocerin, and the stabilizer PYR.

Boronic esters are known for their facile hydrolysis, generating products, such as boronic acids and alcohols, which are in general considered nontoxic and do not lead to drastic pH changes in the body.[29] Therefore, research was conducted to determine whether boronic ester-based monomers are suitable to generate highly degradable networks, which can be structured via SLA printing and comprise mechanical properties sufficient to replace hard bony tissue.

3.1. Synthesis of Monomers and Thiols for Degradable Networks. To demonstrate that boronic esters can be used for the fabrication of degradable materials with potential use in BTE, certain key characteristics of formulation components had to be considered. As the first model compound, we chose the boronic ester ADB (Figure 1), which comprises a cyclic and aromatic structure and the potential of cleavage at two boronic ester bonds. This monomer was recently described to undergo thiol−ene photopolymerization under the formation of polymers used for self-healing, reprocessing, and shape memory, which were also shown to be hydrolyzable.[47,55] Nevertheless, all formed materials exhibited insufficient mechanical properties, as well as significant creep and drastic swelling upon hydrolysis, making them unsuitable for degradable bone replacement materials. As a result, we envisioned the novel monomer structure of VDB (Figure 1), with a shorter, less-flexible side chain. Compared to ADB, this literature-unknown molecule promises to generate degradable networks with enhanced mechanical properties, which may confine hydrolysis of the network to the surface, thereby enabling the desired surface erosion behavior.

Both boronic esters were easily prepared by condensation of the aromatic diboronic acid and corresponding diols (Scheme 1a). The synthesis, adapted from Chen et al.,[40] proceeds very smoothly under mild conditions in THF by removal of the formed water with a drying agent. Full conversion was confirmed after a few hours, and no formation of any side products was observed. Hence, both products could be obtained in quantitative yields.

For means of comparison, a nondegradable reference was used, namely, difunctional VSA (Figure 1). This compound is a commercial monomer and is described for use in biomedical applications, such as nondegradable hydroxyapatite-filled orthopedic implants[56] or dental restoratives[57] with low shrinkage.

To generate homogeneous and tough networks and to enhance the polymerization rates for 3D structuring, we polymerized the allyl monomers via thiol−ene chemistry. Because degradation should not be influenced by the thiol, we chose the compound TMT (Figure 1), which is a low-odor thiol used in dental applications[50,51] and does not contain any hydrolyzable bonds, such as ester groups, typically found in commercial thiols. Furthermore, due to its rigid structure, the mechanical properties of the resulting materials should be enhanced. The thiol was synthesized in a two-step procedure described by Reinelt et al.[50,51] by the radical addition of thioacetic acid and subsequent hydrolysis to the target compound under acidic conditions and could be obtained in high yields of 93% (Scheme 1b).

3.2. Cytotoxicity. Photopolymers used *in vivo* pose the risk of releasing unreacted monomers into the surrounding media. Hence, determination of the influence of used building blocks on cell proliferation and differentiation is crucial. To retrieve this information, cell viability tests were conducted with mouse cells (NCTC Clone 929), which were incubated for 24 h with

https://doi.org/10.1021/acsapm.3c01000
ACS Appl. Polym. Mater. 2023, 5, 5758−5771

Scheme 1. (a) Synthesis of Boronic Ester Monomers for Hydrolytically Degradable Polymer Networks and (b) Synthesis of the Trifunctional Cross-Linker TMT

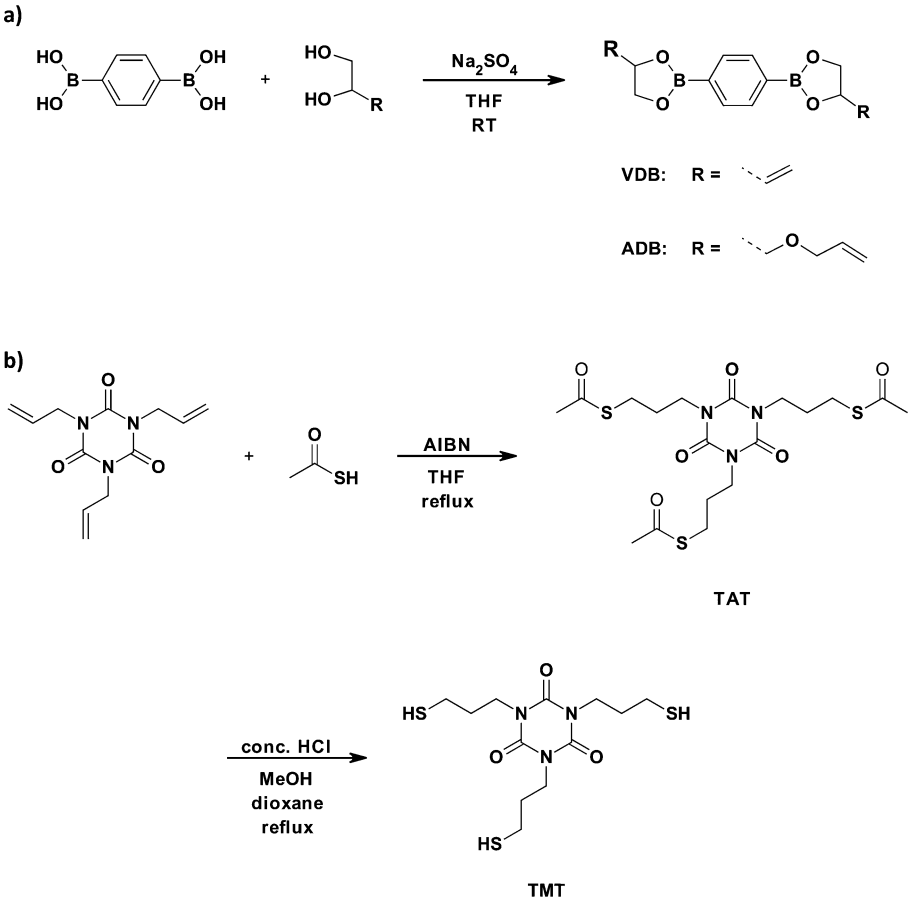

varying concentrations of the monomers and the used thiol. The concentrations ranged from 2.5 to 10 mmol/L. A qualitative microscopic assessment of the cells revealed no morphological changes caused by the substances (Figure S4). The concentration at which 50% of the cells are still viable after the incubation time (EC_{50}) was used for quantitative assessment of the cytotoxicity of the compounds (Table 1). The exact cell viabilities at the different substance concentrations are given in Table S1).

Table 1. Cytotoxicity (EC_{50} Values) of Novel Boronic Ester Monomers VDB, ADB, and VSA and the Thiol Cross-Linker TMT

substance	EC_{50} (mM)
VDB	>10
ADB	2.5
VSA	>10
TMT	2.5

EC_{50} values of all compounds range from 2.5 to >10 mM. Compared to difunctional (meth)acrylates, i.e., 1,4-butane-diol diacrylate and 1,4-butanediol dimethacrylate with reported EC_{50} of <0.16 mM and 1.3 mM[3], all tested compounds demonstrated significantly better tolerance by the cells. This clearly shows that all monomers and thiols used within these studies exert sufficiently low toxic effects on the fibroblast cells. It is noteworthy that the novel boronic ester VDB is less toxic than the methacrylate reference by a factor of 8 and even 2 orders of magnitude less toxic than 1,4-butanediol diacrylate. Furthermore, its EC_{50} is as high as that for the reference VSA (>10 mM), which further supports the excellent biocompatibility of this compound, as VSA is patented for several biomedical applications.[56,57]

3.3. Network Formation. To prepare polymer networks, the different dienes were photopolymerized with the trifunctional cross-linker TMT with 1 wt % photoinitiator (Ivocerin; Figure 1) in an equimolar ratio of vinyl-to-thiol groups of 1:1. Scheme 2 shows the network formation with the boronic ester VDB. Both boronic ester monomers were solids at rt. Due to the insolubility of the monomer VDB in the thiol TMT at rt, formulations had to be analyzed at 55 °C. For means of comparison, ADB and VSA, which were soluble in the thiol at rt, were also photopolymerized at this temperature. To mitigate potential disadvantages of thiol−ene chemistry, such as poor storage stability, 0.02 wt % PYR (Figure 1) was added prior to photopolymerization as a radical inhibitor to all resin mixtures. With the addition of this stabilizer, the formulations showed no notable change in viscosity at 55 °C over the course of 8 h, which is a typical time span used for 3D printing of larger objects.

All formulations exhibited low viscosities of <0.8 Pa·s (Table S1) at 25 and 55 °C, which is far below the maximum processing viscosity of SLA of 20 Pa·s.[58]

For the intended application in 3D printing, parameters such as the reactivity and chemical conversion during photopolymerization are crucial. These key values can be determined with *in situ* RT-NIR photorheology.[59] The time until gelation

https://doi.org/10.1021/acsapm.3c01000
ACS Appl. Polym. Mater. 2023, 5, 5758−5771

Scheme 2. Network Formation of the Difunctional Boronic Ester VDB and the Trifunctional Thiol TMT and Subsequent Surface Erosion Mechanism of This Network, with the Sample Decreasing in Size as a Function of Time while Maintaining Structural Integrity

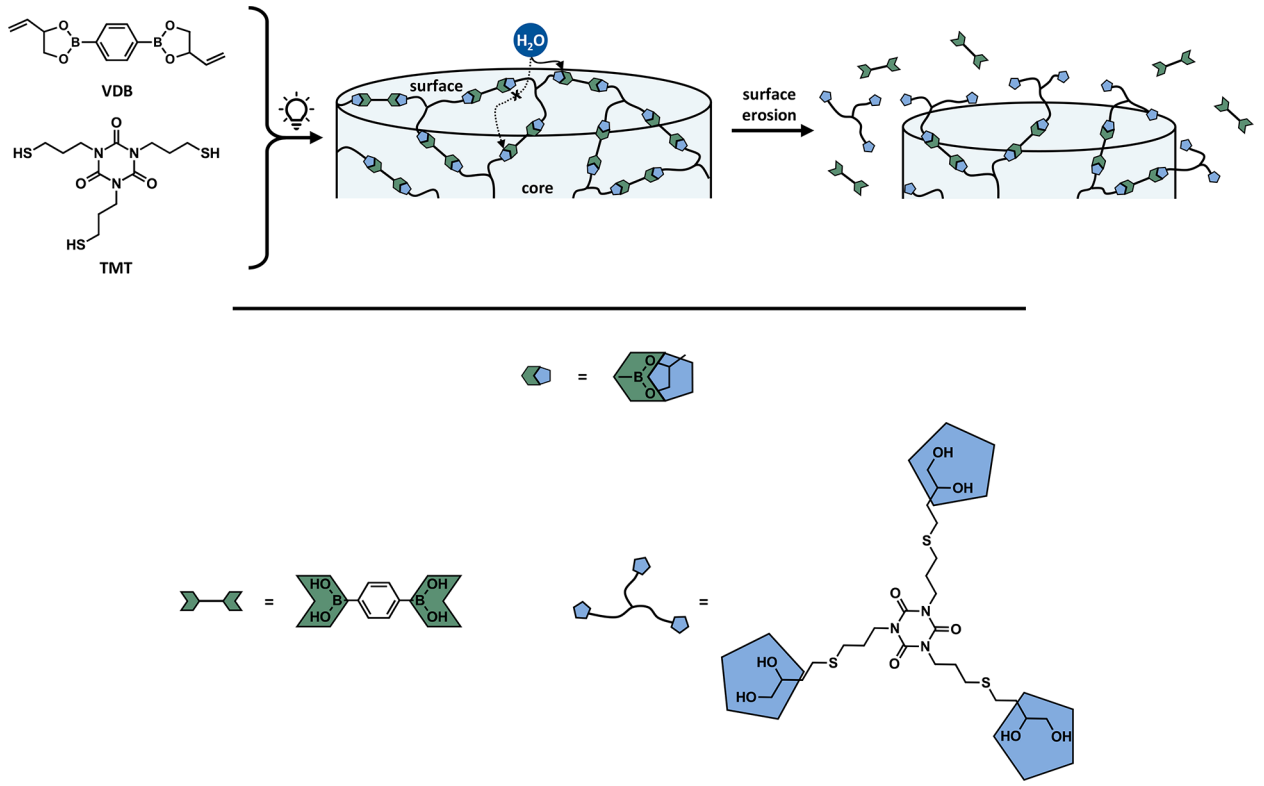

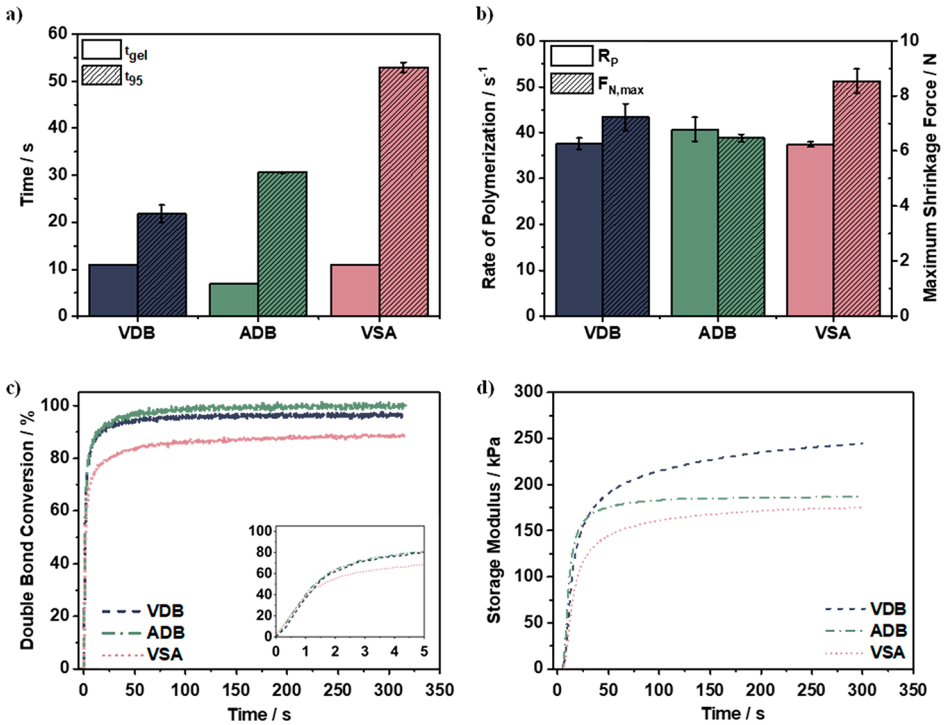

Figure 2. Results of photorheological analysis of formulations containing VDB (blue), ADB (green), or VSA (pink) and the cross-linking thiol TMT in an equimolar ratio of double bonds to thiol groups at 55 °C: (a) obtained values for the time to reach the gel point t_{gel} (no pattern) and the time to reach 95% of the overall conversion t_{95} (striped pattern); (b) obtained results for the rate of polymerization R_P (no pattern) and absolute values for $F_{N,max}$ (striped pattern); (c) comparison of the exemplary curves of DBC of the whole measurement and initiation phase (inlay); (d) comparison of the exemplary curves of the storage modulus over time of the monomers VDB (dashed), ADB (dash-dotted), and VSA (dotted) with the thiol TMT.

https://doi.org/10.1021/acsapm.3c01000
ACS Appl. Polym. Mater. 2023, 5, 5758−5771

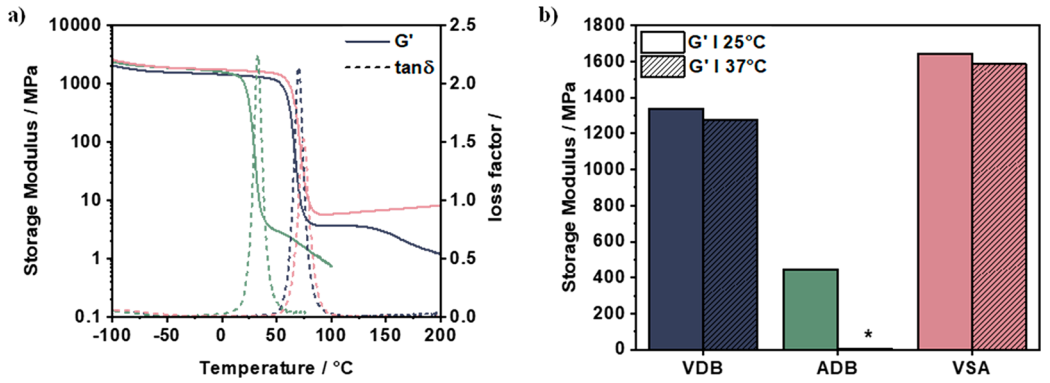

Figure 3. (a) Storage modulus (left, full line) and tan δ (right, dashed line) versus temperature: VDB-based (blue) and ADB-based (green) networks compared to VSA-based networks (pink). (b) Storage modulus (right) at 25 °C (no pattern) and 37 °C (striped pattern) of VDB-based (blue) and ADB-based (green) networks compared to VSA-based networks (pink). *A low $G'_{37\ °C}$ of 5 MPa was obtained for the ADB-based network.

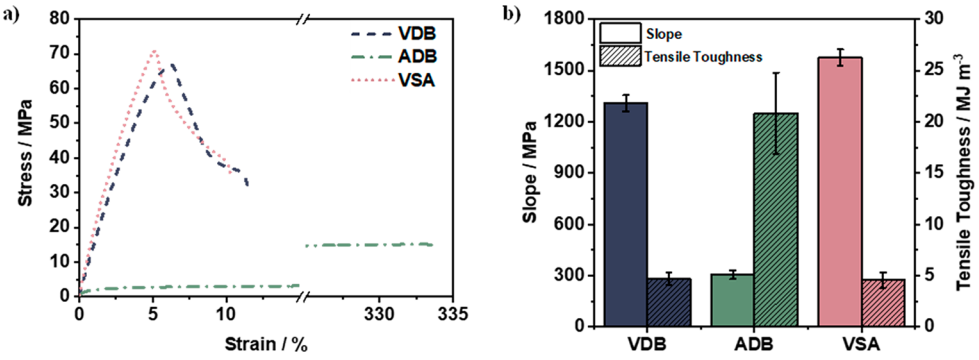

Figure 4. (a) Tensile curves of VDB-based (blue, dashed), ADB-based (green, dotted), and VSA-based (pink, dash-dotted) networks. (b) Slope of the testing curve and tensile toughness calculated by integration of the tensile curves of VDB-based (blue), ADB-based (green), and VSA-based (pink) networks.

t_{gel} (intersection of the storage modulus G' and the loss modulus G'') should be as low as possible because it determines the minimum irradiation time required to generate one object layer. Furthermore, high final double-bond conversions (DBC_{final}) at the end of the curing process are necessary to achieve good mechanical properties. A low time to attain 95% of the final observed conversion (t_{95}) is favorable for building objects with sufficient speed because the previous layer needs a certain stability before the next layer can be deposited to avoid failure during printing. Last, the occurring shrinkage stress, which correlates with the maximum normal force ($F_{N,max}$) should be as low as possible to avoid residual internal stress or even cracks within the printed structures.[8,59] The results are listed in Figure 2. Numerical data obtained in these measurements can be found in Table S4. Detailed data obtained for formulations containing ADB and VSA at 25 °C are given in Table S3 and Figure S5.

All formulations exhibit similar R_p values of 37−41%/s and similar times until gelation (7−11 s) at 55 °C, which demonstrates high photoreactivity and fast cross-linking, despite the employment of thiols as network modifiers, which typically delays the gel point.[17,60−62] Additionally, high DBC_{final} values of >95% were reached in photopolymerizations with both boronic ester monomers, guaranteeing a low amount of residual low-molecular-weight components inside the polymer networks. Slightly lower but still high conversions of 89% were obtained with the reference VSA, which is due to the short monomer structure, leading to a higher cross-linking density and hence reduced monomer mobility during network formation. Furthermore, boronic ester-containing monomers positively impact shrinkage during polymerization because significantly lower maximum shrinkage forces (decreases of 15% for VDB and 25% for ADB compared to VSA) were observed in these systems. This is most likely the result of a certain amount of transesterification reactions of the boronic ester bonds at the elevated temperature of 55 °C, which leads to network rearrangement during curing. Hence, next to higher final conversions, boronic ester monomers also act as potent shrinkage-reducing additives. The highest final storage modulus was obtained with VDB (240 kPa), while significantly lower values were shown for ADB (191 kPa) and VSA (170 kPa). This demonstrates the importance of the short and rigid monomer structure of VDB, which in combination with the higher conversions results in stiffer networks compared to the reference molecules.

3.4. Network Characterization. Bone regeneration scaffolds require certain mechanical properties to provide functional support during bone regeneration, such as high modulus, strength, and toughness.[54] Key parameters such as the storage modulus (G') of the networks at rt and body temperature and the glass transition temperature (T_g) were analyzed by DMTA. The results are summarized in Figure 3. The numerical data are shown in Table S5.

For the ADB-containing network, at 37 °C, the modulus already declined to 5 MPa due to the lowest T_g observed at 33 °C. This value can be explained by the higher length and

https://doi.org/10.1021/acsapm.3c01000
ACS Appl. Polym. Mater. 2023, 5, 5758−5771

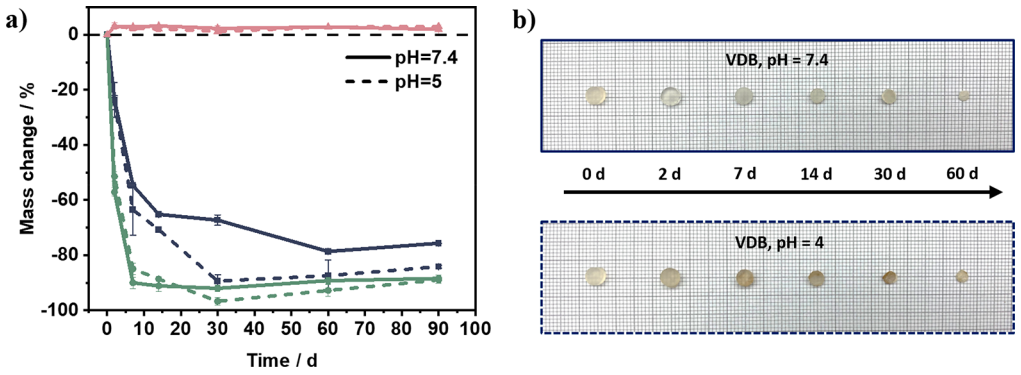

Figure 5. (a) Mass change versus time of polymer networks under physiological conditions (PBS, pH 7.4, solid line) and acidic conditions (acetate buffer, pH 4, dashed line) for thhe VDB-based (blue), ADB-based (green), and reference VSA-based (pink) networks. (b) Photographs of the VDB-based network at different degradation times under physiological conditions (PBS, pH 7.4, upper photograph) and acidic conditions (acetate buffer, pH 4, lower photograph) depicting the surface erosion degradation behavior.

flexibility of the monomer compared to VDB and VSA, resulting in a lower network cross-link density. Hence, this material does not provide sufficient stiffness at 37 °C. In contrast, a high T_g significantly above body temperature was determined for the VDB-based network (70 °C) containing the novel boronic ester monomer, comparable to the T_g value of the reference network containing VSA (74 °C). These values are exceedingly high, considering that these polymer networks are formed with equimolar amounts of thiol, which typically results in low T_g and modulus due to the flexible thioether bridges. Additionally, similar storage moduli at 25 °C were shown for the VDB-based network (1330 MPa) and the reference material (1640 MPa), demonstrating the high stiffness of both networks. The same trends were observed at 37 °C, making the material derived from the novel boronic ester highly promising for applications in the field of BTE. Additionally, no rubbery plateau but a thermoplastic flow behavior was observed for both materials based on boronic esters, which again supports the assumption that these networks exhibit dynamic character due to transesterification reactions, especially observed at elevated temperatures above T_g.

Tensile tests were conducted to gain further insights into crucial mechanical properties, such as tensile strength, strain at break, and tensile toughness, which can be obtained by integration of the testing curve. Because no extensometer was used, the slope in the linear regime of the curves was used to evaluate the materials' stiffness. The results are shown in Figure 4. The numerical data are tabulated in Table S6.

A high strength of >65 MPa and a comparably good strain at break of >10% and tensile toughness of >4 MJ/m^3 were observed for the VDB-based network and the reference material containing VSA, demonstrating the importance of rigid, short monomer structures on enhanced network properties. A slightly stronger slope of the linear curve progression, corresponding to higher stiffness, was observed with networks containing VSA (1580 MPa) compared to VDB (1310 MPa), which again can be explained by the higher cross-linking density due to the shorter monomer structure. This is corroborated by the mechanical properties of networks composed of ADB. Although a highest tensile toughness of 20.8 MJ/m^3 was determined, this is due to the high strain at break (313%) because a very low stiffness and tensile strength of 14.6 MPa is exhibited by this material. This again is due to the flexible and longer monomer structure, leading, in turn, to a reduced cross-link density and network softening.

3.5. Degradation of Boronic Ester-Containing Networks. Current state-of-the-art photopolymers used for the production of 3D-printed regeneration scaffolds, including poly[(meth)acrylates], poly(vinyl esters), and poly(vinyl carbonates), display certain disadvantages, such as unfavorable degradation via bulk erosion or insufficient degradation speed *in vivo*.[1,3,9,10] Compared to carbon-based esters, boronic esters are readily hydrolyzed without the addition of catalyst. Additionally, the boronic acids formed upon hydrolysis act as mild Lewis acids and do not lead to drastic pH changes in the surrounding medium.[28−30] Due to these advantages, monomers containing boronic ester bonds might be suitable to generate materials degrading via surface erosion, during which material loss is confined to the surface and structural integrity of the implant is maintained.[6,11]

To study whether the new type of boronic ester monomer can not only provide the material with good mechanical properties but also enhance the degradation behavior of polymer networks, *in vitro* hydrolytic degradation studies were performed under physiological conditions (37 °C, PBS buffer, pH 7.4) as well as acidic conditions (37 °C, acetate buffer, pH 4). The latter was used to mimic the conditions during bone regeneration because an acidic pH below 4.5 is essential for osteoclast-driven bone resorption.[26] Although not relevant for conditions *in vivo*, degradation was also studied in a basic buffer medium (37 °C, carbonate−bicarbonate buffer, pH 10) to determine possible differences to the aforementioned conditions (Table S10). Degradation was monitored over a period of 3 months by measuring the swelling weight and mass of the samples after drying to determine both network swelling and mass change.

Figure 5 shows the results. The results for the swelling of the samples are shown in Figure S6, and all numerical data are provided in Tables S7−S10.

The reference system containing VSA shows no signs of degradation during the testing period but a slight amount of irreversible water uptake (2−3%), which is also reflected in slightly negative swelling values (Table S9). Hence, this reference monomer is nondegradable, and the spiroacetal moieties are not hydrolyzed under neutral or acidic conditions. This is also shown by the samples, which do not display any change in size as a function of time (Figure S7).

https://doi.org/10.1021/acsapm.3c01000
ACS Appl. Polym. Mater. 2023, 5, 5758−5771

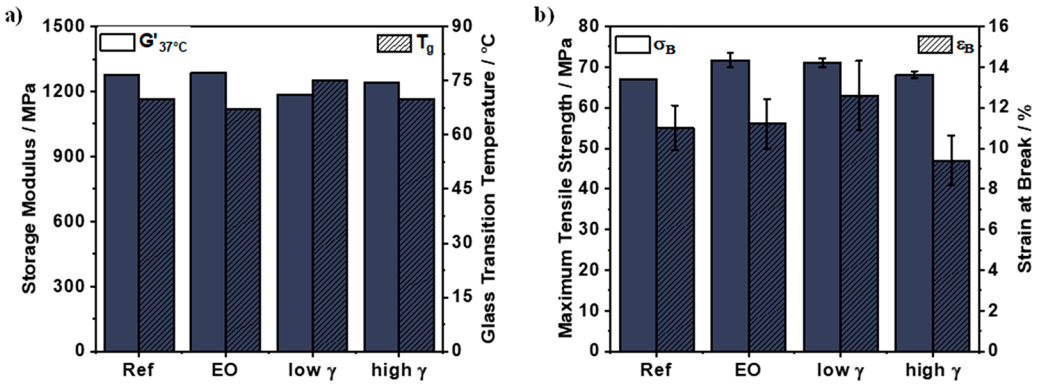

Figure 6. Results of the mechanical properties of nonsterilized (ref) and sterilized VDB-based materials (blue) with EO, low doses of γ radiation (low γ), or high doses of γ radiation (high γ): (a) storage modulus at 37 °C (left, no pattern) and glass transition temperature (right, striped pattern); (b) maximum tensile strength (left, no pattern) and strain at break (right, striped pattern).

For boron-containing systems, no swelling was observed over the course of the experiment, with determined values close to 0% (Tables S7 and S8). Regarding mass change, a different behavior was observed compared to VSA. Because boronic ester bonds reside at every cross-linking point, total material dissolution was expected. Nevertheless, note that no total degradation of the polymers was determined during the testing period. Instead, slight traces of solid residues were observed at the bottom of the vials after drying to a constant weight, attributed to slight traces of hydrolysis products, residual material, and buffer salts in the testing vials.

For the networks containing ADB, no material could be removed from the vials after 2 days because disruption of the samples occurred under both conditions. This shows that hydrolysis of the network occurs very fast due to the rather low network T_g of 33 °C. Because this temperature is lower than the conditions applied in the studies, water can penetrate the network easily due to the high chain mobility of the network. Mass change values show the same trends with an erosion of 85−90% after 7 days, and only a slight further reduction (88−96%) was observed for the remaining testing period. Hence, this system is more suitable for applications requiring low T_g values and fast degradation rates within 2−7 days, such as drug-delivery vehicles.

For the network containing VDB, an immediate onset of degradation was shown, followed by an exponential decay of the mass, with mass changes of 79% and 87% after 60 days under neutral and acidic conditions, respectively. After 90 days, no samples could be removed because only very thin and fragile samples were observed at the bottom of the vials.

Figure 5b provides insight into the degradation mechanism of networks based on the VDB under neutral and acidic conditions. It is shown that a general retention of the shape occurs, which decreases in size as a function of the degradation time, which is characteristic for a surface erosion process. This shows the importance of the high T_g and tensile strength of this material because this results in reduced chain mobility at the degradation temperature. This, in turn, prevents the diffusion of water into the samples and confines hydrolysis to the surface.

To study the hydrolysis products and residues, each buffer solution was extracted with $CDCl_3$ after 3 months and analyzed by NMR. The spectra are given in Figures S8−S13. Mainly water was detected, demonstrating that all degradation products are water-soluble, which is an important prerequisite for metabolization or elimination via the liver or kidneys.[16,21−23]

3.6. Influence of Sterilization on the Mechanical Properties. The material containing the novel boronic ester VDB combines superior mechanical properties with fast and favorable degradation. Nevertheless, for applications *in vivo*, the sterility of the implant needs to be guaranteed to minimize the risk of infection or immune responses. In general, several sterilization methods are known for medical materials, with exposure to gaseous chemicals, such as EO, or γ radiation being the most relevant for the materials studied here.[63−65] Nevertheless, application of these methods, above all the exposure to high doses of γ-rays, may cause irreversible structural changes in the polymer network, possibly causing an altering of the mechanical properties of the material and thereby premature implant failure.[66]

To study the influence of sterilization on the most promising material containing VDB, the networks were subjected to sterilization with EO (6% EO, 55 °C, 2 h), the lowest possible dosage of γ radiation still considered sufficient for sterilization of medical implants (18 kGy, 5 h), or high γ-radiation dosage (~31 kGy, 5 h), and mechanical properties were determined prior to (reference, ref) and after application of each method (EO, low γ, or high γ) via DMTA and tensile tests. Figure 6 shows the results, and the numerical data are provided in Tables S8 and S11.

High T_g (67−75 °C) and $G'_{37\,°C}$ (1230−1340 MPa) were obtained for all sterilized materials, with a slight increase of 5 °C for the network exposed to low γ-radiation doses compared to the nonsterilized reference. This was corroborated by the tensile tests, confirming that high strengths (67−72 MPa) and good strains at break (9−13%) were maintained, with only a minor decrease in strain of 2% at high γ dosage compared to the reference. This demonstrates that the applied sterilization techniques do not cause altering of the network, and even high doses of γ radiation can be applied without significantly influencing the excellent mechanical properties of the VDB-based material and thereby guaranteeing sterility of scaffolds intended for the use *in vivo*.

3.7. 3D Printing. Because the polymer containing the novel boronic ester VDB displayed not only excellent mechanical properties but also enhanced degradation via the desired surface erosion behavior, 3D structuring of the resin was conducted to confirm its applicability in the production of patient-specific implants. To enhance the printing resolution,

https://doi.org/10.1021/acsapm.3c01000
ACS Appl. Polym. Mater. 2023, 5, 5758−5771

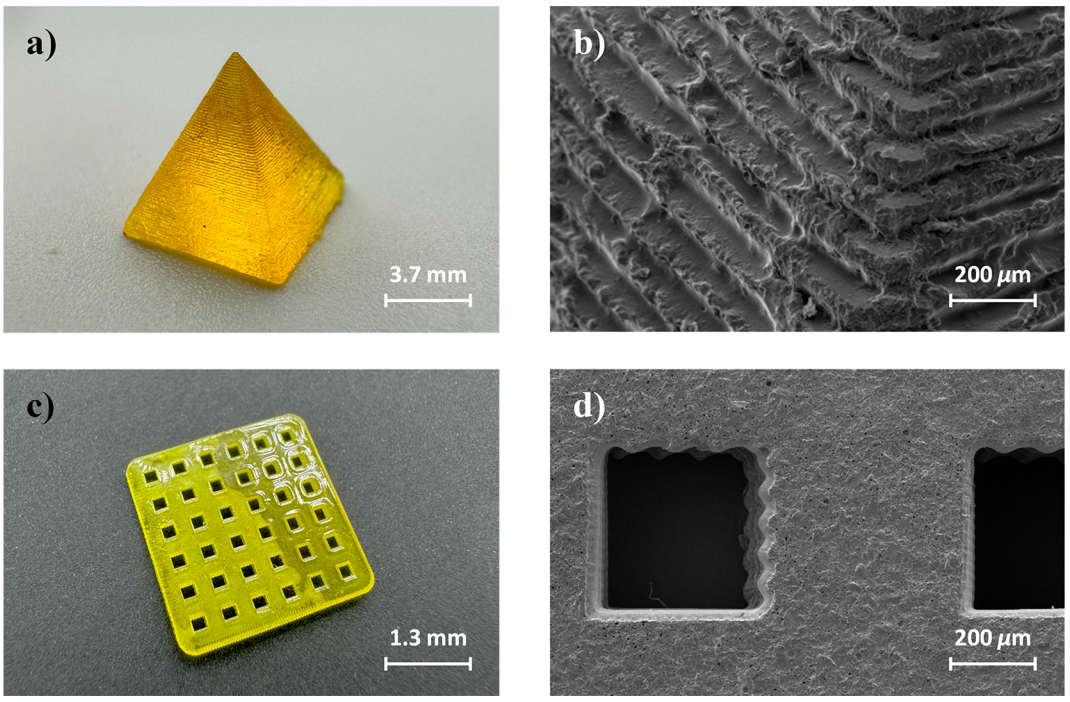

Figure 7. Photography of the (a) 3D-printed pyramid and (c) porous structure with pore diameters of 200 μm from the VDB-based formulation. (b and d) SEM imaging.

the absorber QY was added to the formulation. For this absorber, it was shown that increasing concentration led to not only enhanced control over the curing depth but also increased mechanical properties of layers, when applied in thiol−ene systems.[67] As a proof of concept, a pyramid object with a square base of 7.3 × 7.3 mm^2 was structured in a layer-by-layer approach via a laser at 55 °C (details in the Experimental Section and Figure 7a; 100 μm layer thickness). To prove that printing of more complex structures is feasible, a porous structure with a square base of 3.2 × 3.2 mm^2 and pore diameters of 200 μm, which were previously shown to provide the ideal balance between cell attachment and bone growth in regeneration scaffolds by Murphy et al.,[68] was printed as well. SEM images (Figure 7b,d) visualize the successful printing process with an achieved curing depth of 125 μm per layer for both objects, which demonstrates the high resolution obtained with SLA. High selectivity of the photocuring reaction due to the lack of light-induced or diffusional overpolymerization validates the applicability of this degradable thiol−ene system for the future fabrication of more complex structures. Most importantly, due to the high T_g of the formed polymers, no creep was observed during the printing process. Hence, no addition of a monomer without boronic ester bonds was necessary, as previously reported for the 3D printing of resins containing boronic esters.[47]

Additionally, long-term creep experiments were conducted at body temperature, which showed that materials derived from VDB display significantly lower initial elongation at a load of 1 MPa (Figure S14) and, as the load progresses over time, a significantly lower steady-state creep rate (Table S13) and higher stability compared with ADB-based materials. This higher resistance toward creep was also shown in the creep compliance curves over time (Figure S15). Hence, these tests further demonstrate the importance of using rigid boronic ester monomers in bone replacement materials because, compared to more flexible state-of-the-art monomers, premature loosening of implants may be avoided.

4. CONCLUSIONS

L-AMTs have gained tremendous interest for the production of biocompatible and biodegradable 3D-cellular scaffolds for TE. However, photopolymers derived from state-of-the-art (meth)acrylates, vinyl esters, or vinyl carbonates display disadvantages such as cytotoxicity of residual monomers, undesirable degradation behavior, or insufficient speed of degradation *in vivo*. Therefore, we have examined monomers containing boronic ester bonds as a suitable alternative.

Besides easy synthesis, significantly lower cytotoxicity of the novel allyl ether VDB was shown compared to that of (meth)acrylates, while sufficiently high photoreactivity was maintained. It was shown that, due to facile hydrolysis of the boronic ester bond, this rigid boronic ester monomer is a suitable degradation enhancer, leading to materials with high strength, tensile toughness, and glass transition temperature, which display accelerated degradation via surface erosion under physiological and acidic conditions, which are present during bone remodeling, and may also be sterilized via several methods without forfeiting these properties. Finally, the results demonstrate that a combination of excellent mechanical properties and degradation behavior is possible with careful monomer design.

As a first group, we demonstrated that these monomers can be applied in SLA printing to print porous, degradable, patient-specific bone regeneration scaffolds in the near future. Furthermore, we showed that printing of this binary thiol−ene system without the addition of any nonhydrolyzable monomers is possible due to the enhanced mechanical properties of the polymers, as the dimensional stability during printing is maintained. As a result, networks cleavable at every cross-linking point were obtained, which displayed enhanced

https://doi.org/10.1021/acsapm.3c01000
ACS Appl. Polym. Mater. 2023, 5, 5758−5771

degradation behavior compared to state-of-the-art methacrylate-based systems; hence, the inclusion of hydrolyzable crosslinks into a thiol−ene resin is a powerful strategy to produce 3D-printed bone regeneration scaffolds in the future.

Future work will be done to move beyond *in vitro* analyses and determine long-term local tissue responses and *in vivo* toxicity of these materials in animal models. Furthermore, filling of the materials, i.e., with hydroxyapatite, will be conducted to further tune the network degradation behavior.

■ ASSOCIATED CONTENT

Supporting Information

The Supporting Information is available free of charge at https://pubs.acs.org/doi/10.1021/acsapm.3c01000.

^{1}H, ^{13}C, and ^{11}B NMR spectra of the novel monomer VDB, rheological properties of formulations containing the different monomers and the thiol TMT, detailed results of the RT-NIR photorheology measurements, DMTA measurements, and tensile tests, equations for calculation of the swelling and mass change, swelling versus time of all polymer networks, detailed results of *in vitro* degradation studies, photographs of the VSA-based reference network over time, results of degradation under basic conditions, ^{1}H NMR spectra of buffer solutions extracted with $CDCl_3$, and detailed results of the sterilization studies (PDF)

■ AUTHOR INFORMATION

Corresponding Author

Stefan Baudis − *Christian Doppler Laboratory for Advanced Polymers for Biomaterials and 3D Printing, 1060 Vienna, Austria; Institute of Applied Synthetic Chemistry, Technische Universität (TU) Wien, 1060 Vienna, Austria; Austrian Cluster for Tissue Regeneration, 1200 Vienna, Austria;* orcid.org/0000-0002-5390-0761; Email: stefan.baudis@tuwien.ac.at

Authors

Lisa Sinawehl − *Christian Doppler Laboratory for Advanced Polymers for Biomaterials and 3D Printing, 1060 Vienna, Austria; Institute of Applied Synthetic Chemistry, Technische Universität (TU) Wien, 1060 Vienna, Austria; Austrian Cluster for Tissue Regeneration, 1200 Vienna, Austria*

Raffael Wolff − *Institute of Applied Synthetic Chemistry, Technische Universität (TU) Wien, 1060 Vienna, Austria;* orcid.org/0000-0001-5428-5871

Thomas Koch − *Institute of Materials Science and Technology, Technische Universität (TU) Wien, 1060 Vienna, Austria*

Jürgen Stampfl − *Institute of Materials Science and Technology, Technische Universität (TU) Wien, 1060 Vienna, Austria;* orcid.org/0000-0002-3626-5647

Robert Liska − *Institute of Applied Synthetic Chemistry, Technische Universität (TU) Wien, 1060 Vienna, Austria; Austrian Cluster for Tissue Regeneration, 1200 Vienna, Austria*

Complete contact information is available at: https://pubs.acs.org/10.1021/acsapm.3c01000

Author Contributions

S.B. conceived the original idea, designed the research question, and supervised the project. R.L. helped to supervise the project. L.S. developed the experimental methodology, conducted the experiments, data analysis, and data plotting, and wrote the manuscript. J.S. provided the 3D printer, and R.W. performed printing. T.K. conducted SEM measurements and helped to interpret the results. All authors read, discussed, and approved of the final manuscript.

Funding

Funding by the Christian Doppler Research Association within the framework of the "Christian Doppler Laboratory for Advanced Polymers for Biomaterials and 3D Printing" and financial support by the Austrian Federal Ministry for Digital and Economic Affairs and the National Foundation for Research, Technology and Development are gratefully acknowledged.

Notes

The authors declare no competing financial interest.

■ ACKNOWLEDGMENTS

The authors acknowledge Ivoclar Vivadent AG for providing reference materials and TU Wien Bibliothek for financial support through its Open Access Funding Program. Special thanks to Adem Aksu and Frank Reinauer for performing sterilization of the materials at KLS Martin Group and Roman Lieber and Barbara Kapeller for conducting *in vitro* cytotoxicity studies at Medizinische Universität Wien.

■ REFERENCES

(1) Heller, C.; Schwentenwein, M.; Varga, F.; Stampfl, J.; Liska, R. Additive Manufacturing Technologies for the 3D Fabrication of Biocompatible and Biodegradable Photopolymers. *Mater. Res. Soc. Symp. Proc.* **2009**, *1239* (1), 805.

(2) Ligon, S. C.; Liska, R.; Stampfl, J.; Gurr, M.; Mulhaupt, R. Polymers for 3D Printing and Customized Additive Manufacturing. *Chem. Rev.* **2017**, *117* (15), 10212−10290.

(3) Heller, C.; Schwentenwein, M.; Russmueller, G.; Varga, F.; Stampfl, J.; Liska, R. Vinyl Esters: Low Cytotoxicity Monomers for the Fabrication of Biocompatible 3D Scaffolds by Lithography Based Additive Manufacturing. *J. Polym. Sci. Pol Chem.* **2009**, *47* (24), 6941−6954.

(4) Becker, S. T.; Bolte, H.; Krapf, O.; Seitz, H.; Douglas, T.; Sivananthan, S.; Wiltfang, J.; Sherry, E.; Warnke, P. H. Endocultivation: 3D printed customized porous scaffolds for heterotopic bone induction. *Oral Oncol* **2009**, *45* (11), e181−8.

(5) Neves, S. C.; Mota, C.; Longoni, A.; Barrias, C. C.; Granja, P. L.; Moroni, L. Additive manufactured polymeric 3D scaffolds with tailored surface topography influence mesenchymal stromal cells activity. *Biofabrication* **2016**, *8* (2), 025012.

(6) Davison, N. L.; Barrère-de Groot, F.; Grijpma, D. W. Degradation of Biomaterials. In. *Tiss Eng.* **2014**, 177−215.

(7) Ware, T.; Jennings, A. R.; Bassampour, Z. S.; Simon, D.; Son, D. Y.; Voit, W. Degradable, silyl ether thiol-ene networks. *Rsc Adv.* **2014**, *4* (75), 39991−40002.

(8) Orman, S.; Hofstetter, C.; Aksu, A.; Reinauer, F.; Liska, R.; Baudis, S. Toughness enhancers for bone scaffold materials based on biocompatible photopolymers. *J. Polym. Sci. Pol Chem.* **2019**, *57* (2), 110−119.

(9) Husár, B.; Heller, C.; Schwentenwein, M.; Mautner, A.; Varga, F.; Koch, T.; Stampfl, J.; Liska, R. Biomaterials based on low cytotoxic vinyl esters for bone replacement application. *J. Polym. Sci. Pol Chem.* **2011**, *49* (23), 4927−4934.

(10) Mautner, A.; Steinbauer, B.; Orman, S.; Russmuller, G.; Macfelda, K.; Koch, T.; Stampfl, J.; Liska, R. Tough Photopolymers Based on Vinyl Esters for Biomedical Applications. *J. Polym. Sci. Pol Chem.* **2016**, *54* (13), 1987−1997.

(11) Alameda, B. M.; Palmer, T. C.; Sisemore, J. D.; Pierini, N. G.; Patton, D. L. Hydrolytically degradable poly(β-thioether ester ketal)

thermosets via radical-mediated thiol−ene photopolymerization. *Polym. Chem.* **2019**, *10* (41), 5635−5644.
(12) Heller, C.; Schwentenwein, M.; Russmuller, G.; Koch, T.; Moser, D.; Schopper, C.; Varga, F.; Stampfl, J.; Liska, R. Vinylcarbonates and Vinylcarbamates: Biocompatible Monomers for Radical Photopolymerization. *J. Polym. Sci. Pol Chem.* **2011**, *49* (3), 650−661.
(13) Mautner, A. Development of Low Cytotoxic Photopolymers. Thesis, TU Wein, Vienna, Austria, 2012.
(14) Mautner, A.; Qin, X.; Kapeller, B.; Russmueller, G.; Koch, T.; Stampfl, J.; Liska, R. Efficient curing of vinyl carbonates by thiol-ene polymerization. *Macromol. Rapid Commun.* **2012**, *33* (23), 2046−52.
(15) Mautner, A.; Steinbauer, B.; Russmuller, G.; Lieber, R.; Koch, T.; Stampfl, J.; Liska, R. Vinyl carbonate photopolymers with improved mechanical properties for biomedical applications. *Des. Monomers Polym.* **2016**, *19* (5), 437−444.
(16) Henkel, J.; Woodruff, M. A.; Epari, D. R.; Steck, R.; Glatt, V.; Dickinson, I. C.; Choong, P. F.; Schuetz, M. A.; Hutmacher, D. W. Bone Regeneration Based on Tissue Engineering Conceptions - A 21st Century Perspective. *Bone Res.* **2013**, *1* (3), 216−48.
(17) Ligon, S. C.; Seidler, K.; Gorsche, C.; Griesser, M.; Moszner, N.; Liska, R. Allyl sulfides and α-substituted acrylates as addition-fragmentation chain transfer agents for methacrylate polymer networks. *J. Polym. Sci. Pol Chem.* **2016**, *54* (3), 394−406.
(18) Ligon-Auer, S. C.; Schwentenwein, M.; Gorsche, C.; Stampfl, J.; Liska, R. Toughening of photo-curable polymer networks: a review. *Polym. Chem.* **2016**, *7* (2), 257−286.
(19) Hoyle, C. E.; Bowman, C. N. Thiol-ene click chemistry. *Angew. Chem., Int. Ed. Engl.* **2010**, *49* (9), 1540−73.
(20) Reddy, S. K.; Cramer, N. B.; Bowman, C. N. Thiol-vinyl mechanisms. 1. Termination and propagation kinetics in thiol-ene photopolymerizations. *Macromol.* **2006**, *39* (10), 3673−3680.
(21) Ratner, B. D., Hoffman, A. S., Schoen, F. J., Lemons, J. E., Eds. *Biomaterials Science, An Introduction to Materials in Medicine*, 2nd ed.; Elsevier, 2004; p 851 pp.
(22) Heimann, R. B.; Lehmann, H. D. *Bioceramic Coatings for Medical Implants*; Wiley-VCH, 2012.
(23) Nair, L. S.; Laurencin, C. T. Biodegradable polymers as biomaterials. *Prog. Polym. Sci.* **2007**, *32* (8−9), 762−798.
(24) Rehmann, M. S.; Garibian, A. C.; Kloxin, A. M. Hydrolytically degradable thiol-ene hydrogels for protein release. *Macromol. Symp.* **2013**, *329* (1), 58−65.
(25) Heller, J. *Biopolymers I. Advances in Polymer Science, ed.*; Springer, 1993; Vol. *107*.
(26) Dellago, B.; Ricke, A.; Geyer, T.; Liska, R.; Baudis, S. Photopolymerizable precursors for degradable biomaterials based on acetal moieties. *Eur. Polym. J.* **2021**, *154*, 110536.
(27) Chatterjee, S.; Ramakrishnan, S. Hyperbranched Polyacetals with Tunable Degradation Rates. *Macromol.* **2011**, *44* (12), 4658−4664.
(28) Lennox, A. J.; Lloyd-Jones, G. C. Selection of boron reagents for Suzuki-Miyaura coupling. *Chem. Soc. Rev.* **2014**, *43* (1), 412−43.
(29) Hall, D. G. *Boronic Acids: Preparation and Applications in Organic Synthesis and Medicine*; Wiley, 2005.
(30) Brooks, W. L.; Sumerlin, B. S. Synthesis and Applications of Boronic Acid-Containing Polymers: From Materials to Medicine. *Chem. Rev.* **2016**, *116* (3), 1375−97.
(31) Bull, S. D.; Davidson, M. G.; van den Elsen, J. M.; Fossey, J. S.; Jenkins, A. T.; Jiang, Y. B.; Kubo, Y.; Marken, F.; Sakurai, K.; Zhao, J.; James, T. D. Exploiting the reversible covalent bonding of boronic acids: recognition, sensing, and assembly. *Acc. Chem. Res.* **2013**, *46* (2), 312−26.
(32) Deng, C. C.; Brooks, W. L. A.; Abboud, K. A.; Sumerlin, B. S. Boronic Acid-Based Hydrogels Undergo Self-Healing at Neutral and Acidic pH. *ACS Macro Lett.* **2015**, *4* (2), 220−224.
(33) Cai, B.; Luo, Y.; Guo, Q.; Zhang, X.; Wu, Z. A glucose-sensitive block glycopolymer hydrogel based on dynamic boronic ester bonds for insulin delivery. *Carbohydr. Res.* **2017**, *445*, 32−39.
(34) Marco-Dufort, B.; Tibbitt, M. W. Design of moldable hydrogels for biomedical applications using dynamic covalent boronic esters. *Mater. Today Chem.* **2019**, *12*, 16−33.
(35) Brooks, W. L. A.; Deng, C. C.; Sumerlin, B. S. Structure-Reactivity Relationships in Boronic Acid-Diol Complexation. *ACS Omega* **2018**, *3* (12), 17863−17870.
(36) Rottger, M.; Domenech, T.; van der Weegen, R.; Breuillac, A.; Nicolay, R.; Leibler, L. High-performance vitrimers from commodity thermoplastics through dioxaborolane metathesis. *Science* **2017**, *356* (6333), 62−65.
(37) Cromwell, O. R.; Chung, J.; Guan, Z. Malleable and Self-Healing Covalent Polymer Networks through Tunable Dynamic Boronic Ester Bonds. *J. Am. Chem. Soc.* **2015**, *137* (20), 6492−5.
(38) Chen, Y.; Tang, Z.; Zhang, X.; Liu, Y.; Wu, S.; Guo, B. Covalently Cross-Linked Elastomers with Self-Healing and Malleable Abilities Enabled by Boronic Ester Bonds. *ACS Appl. Mater. Interfaces* **2018**, *10* (28), 24224−24231.
(39) Cash, J. J.; Kubo, T.; Dobbins, D. J.; Sumerlin, B. S. Maximizing the symbiosis of static and dynamic bonds in self-healing boronic ester networks. *Polym. Chem.* **2018**, *9* (15), 2011−2020.
(40) Cash, J. J.; Kubo, T.; Bapat, A. P.; Sumerlin, B. S. Room-Temperature Self-Healing Polymers Based on Dynamic-Covalent Boronic Esters. *Macromol.* **2015**, *48* (7), 2098−2106.
(41) Bapat, A. P.; Sumerlin, B. S.; Sutti, A. Bulk network polymers with dynamic B-O bonds: healable and reprocessable materials. *Mater. Horiz* **2020**, *7* (3), 694−714.
(42) Tajbakhsh, S.; Hajiali, F.; Maric, M. Recyclable Polymers with Boronic Ester Dynamic Bonds Prepared by Miniemulsion Polymerization. *Acs Appl. Polym. Mater.* **2021**, *3* (7), 3402−3415.
(43) Chen, Y.; Tang, Z.; Zhang, X.; Liu, Y.; Wu, S.; Guo, B. Covalently Cross-Linked Elastomers with Self-Healing and Malleable Abilities Enabled by Boronic Ester Bonds. *ACS Appl. Mater. Interfaces* **2018**, *10* (28), 24224−24231.
(44) Chen, Y.; Tang, Z. H.; Liu, Y. J.; Wu, S. W.; Guo, B. C. Mechanically Robust, Self-Healable, and Reprocessable Elastomers Enabled by Dynamic Dual Cross-Links. *Macromol.* **2019**, *52* (10), 3805−3812.
(45) Wang, Y. A.; Yu, H. S.; Yang, H. Y.; Hao, X.; Tang, Q.; Zhang, X. Y. An Injectable Interpenetrating Polymer Network Hydrogel with Tunable Mechanical Properties and Self-Healing Abilities. *Macromol. Chem. Phys.* **2017**, *218* (23), 1700348.
(46) Huang, W. W.; Qi, C. Z.; Gao, Y. Injectable Self-Healable Nanocomposite Hydrogels with Mussel Inspired Adhesive Properties for 3D Printing Ink. *Acs Appl. Nano Mater.* **2019**, *2* (8), 5000−5008.
(47) Robinson, L. L.; Self, J. L.; Fusi, A. D.; Bates, M. W.; Read de Alaniz, J.; Hawker, C. J.; Bates, C. M.; Sample, C. S. Chemical and Mechanical Tunability of 3D-Printed Dynamic Covalent Networks Based on Boronate Esters. *ACS Macro Lett.* **2021**, *10* (7), 857−863.
(48) Liu, Y. J.; Tang, Z. H.; Wang, D.; Wu, S. W.; Guo, B. C. Biomimetic design of elastomeric vitrimers with unparalleled mechanical properties, improved creep resistance and retained malleability by metal-ligand coordination. *J. Mater. Chem. A* **2019**, *7* (47), 26867−26876.
(49) Li, L. Q.; Chen, X.; Jin, K. L.; Torkelson, J. M. Vitrimers Designed Both To Strongly Suppress Creep and To Recover Original Cross-Link Density after Reprocessing: Quantitative Theory and Experiments. *Macromol.* **2018**, *51* (15), 5537−5546.
(50) Reinelt, S.; Tabatabai, M.; Fischer, U. K.; Moszner, N.; Utterodt, A.; Ritter, H. Investigations of thiol-modified phenol derivatives for the use in thiol-ene photopolymerizations. *Beilstein J. Org. Chem.* **2014**, *10*, 1733−40.
(51) Reinelt, S.; Tabatabai, M.; Moszner, N.; Fischer, U. K.; Utterodt, A.; Ritter, H. Synthesis and Photopolymerization of Thiol-Modified Triazine-Based Monomers and Oligomers for the Use in Thiol-Ene-Based Dental Composites. *Macromol. Chem. Phys.* **2014**, *215* (14), 1415−1425.
(52) Boaz, N. W.; Falling, S. N.; Moore, M. K. The preparation of enantiomerically pure 3,4-epoxy-1-butene and 3-butene-1,2-diol. *Synlett* **2005**, *2005* (10), 1615−1617.

https://doi.org/10.1021/acsapm.3c01000
ACS Appl. Polym. Mater. 2023, 5, 5758−5771

(53) Pfaffinger, M. Hot Lithography - New Possibilities in Polymer 3D Printing. *Laser Tech J.* **2018**, *15* (4), 45−47.
(54) Seal, B. L.; Otero, T. C.; Panitch, A. Polymeric biomaterials for tissue and organ regeneration. *Mat Sci. Eng. R* **2001**, *34* (4−5), 147−230.
(55) Liu, Z.; Xiao, D. S.; Liu, G. C.; Xiang, H. P.; Rong, M. Z.; Zhang, M. Q. Self-healing and reprocessing of transparent UV-cured polysiloxane elastomer. *Prog. Org. Coat.* **2021**, *159*, 106450.
(56) Jun, N.; Xiao, P.; Zhang, J. *Application of cyclic polyacetal in producing visible light solidifying material for non-degradation orthopaedics renovation or reshaping beauty treatment*; Patent CN101219237A, 2007.
(57) Aurica, C.; Elena, N. L.; Diaconu, A.; Jordana, N.; Nita, T.; Vera, B. *Matrix Copolymer Synthesis for Bio-medical Applications*; Patent RO131478B1, 2015.
(58) Elomaa, L.; Teixeira, S.; Hakala, R.; Korhonen, H.; Grijpma, D. W.; Seppala, J. V. Preparation of poly(epsilon-caprolactone)-based tissue engineering scaffolds by stereolithography. *Acta Biomater* **2011**, *7* (11), 3850−6.
(59) Gorsche, C.; Harikrishna, R.; Baudis, S.; Knaack, P.; Husar, B.; Laeuger, J.; Hoffmann, H.; Liska, R. Real Time-NIR/MIR-Photorheology: A Versatile Tool for the in Situ Characterization of Photopolymerization Reactions. *Anal. Chem.* **2017**, *89* (9), 4958−4968.
(60) Gorsche, C.; Seidler, K.; Harikrishna, R.; Kury, M.; Koch, T.; Moszner, N.; Liska, R. Difunctional vinyl sulfonate esters for the fabrication of tough methacrylate-based photopolymer networks. *Polymer* **2018**, *158*, 149−157.
(61) Gorsche, C.; Seidler, K.; Knaack, P.; Dorfinger, P.; Koch, T.; Stampfl, J.; Moszner, N.; Liska, R. Rapid formation of regulated methacrylate networks yielding tough materials for lithography-based 3D printing. *Polym. Chem.* **2016**, *7* (11), 2009−2014.
(62) Seidler, K.; Griesser, M.; Kury, M.; Harikrishna, R.; Dorfinger, P.; Koch, T.; Svirkova, A.; Marchetti-Deschmann, M.; Stampfl, J.; Moszner, N.; Gorsche, C.; Liska, R. Vinyl Sulfonate Esters: Efficient Chain Transfer Agents for the 3D Printing of Tough Photopolymers without Retardation. *Angew. Chem., Int. Ed. Engl.* **2018**, *57* (29), 9165−9169.
(63) Shintani, H. Ethylene Oxide Gas Sterilization of Medical Devices. *Biocontrol Sci.* **2017**, *22* (1), 1−16.
(64) Lambert, B. J.; Mendelson, T. A.; Craven, M. D. Radiation and ethylene oxide terminal sterilization experiences with drug eluting stent products. *AAPS PharmSciTech* **2011**, *12* (4), 1116−26.
(65) Alvarado, C. J. Sterilization vs. disinfection vs. clean. *Nurs Clin North Am.* **1999**, *34* (2), 483−91.
(66) *Radiation Technology in Emerging Industrial Applications*; International Atomic Energy Agency: Vienna, Austria, 2003.
(67) Hofstetter, C.; Orman, S.; Baudis, S.; Stampfl, J. Combining cure depth and cure degree, a new way to fully characterize novel photopolymers. *Addit Manuf* **2018**, *24*, 166−172.
(68) Murphy, C. M.; O'Brien, F. J. Understanding the effect of mean pore size on cell activity in collagen-glycosaminoglycan scaffolds. *Cell Adh Migr* **2010**, *4* (3), 377−81.

https://doi.org/10.1021/acsapm.3c01000
ACS Appl. Polym. Mater. 2023, 5, 5758−5771